

Plasma Crystals – Structure and Dynamics^{*)}

Alexander PIEL

Institute for Experimental and Applied Physics, Christian-Albrechts-University, D-24098 Kiel, Germany

(Received 31 August 2008 / Accepted 5 January 2009)

This overview describes the confinement and structure of two-dimensional plasma crystals. Phonons and Mach cones in monolayer systems can be used for diagnostic purposes. Three-dimensional plasma crystals are found as multilayer systems or as Yukawa balls. The differences between Coulomb and Yukawa balls are described by means of a simple model. Optical diagnostic methods for studying dynamical phenomena in three-dimensional plasma crystals are discussed.

© 2009 The Japan Society of Plasma Science and Nuclear Fusion Research

Keywords: complex plasma, plasma crystal, strongly coupled system

DOI: 10.1585/pfr.4.013

1. Introduction

The formation of regular arrangements of charged particles in a confining potential well is known for a long time from Thomson's 1904 model of the atom [1]. Wigner, in 1934, suggested that, by correlation effects, electrons in a metal at zero temperature could settle into a body-centered cubic crystal [2]. Ordered structures of electrically charged, micrometer-sized aluminum particles in a Paul trap were reported by Wuerker *et al.* in 1959 [3]. In the 1960s and 70s, charged polymer particles in a colloidal suspension and interacting by screened Coulomb potentials were detected by Bragg scattering to form crystalline structures [4–7]. Ordered Coulomb clusters consisting of a few laser-cooled ions in a Paul trap were reported in 1987 [8, 9]. Systems with large numbers of laser-cooled ions in a Penning trap [10] or a Paul trap [11] exhibited a shell structure as predicted by molecular-dynamics simulations [12–14]. Crystallization in non-neutral plasmas was reviewed in Ref. [15]. The formation of ordered arrangements of micrometer-sized particles (dust) in a gas discharge plasma was predicted by Ikezi in 1986 [16] and such “plasma crystals” were experimentally realized in 1994 [17–19]. Plasma crystals opened a new window into the physics of strongly-coupled systems. Similar to colloidal suspensions, the convenient size of the particles allows direct observation of individual particle motion in a many-particle system. However, particle friction in a plasma can be made so low that dynamic phenomena become accessible which are overdamped in colloidal suspensions. Compared to trapped laser-cooled ions, the large mass (of 3×10^{11} proton masses for a 10 μm diameter polymer particle) reduces all characteristic frequencies into the range $f < 100$ Hz, which is easily accessible with fast videocameras.

author's e-mail: piel@physik.uni-kiel.de

^{*)} This article is based on the invited talk at the 14th International Congress on Plasma Physics (ICPP2008).

This article describes the physical processes that determine the structure and the dynamical properties of two and three-dimensional plasma crystals. Due to the limited space, the discussion emphasizes experimental findings.

2. Plasma Crystals

A plasma crystal is an assembly of electrically charged micrometer-sized particles (“dust”) in a gas discharge plasma. These particles carry a few thousand elementary charges. Under typical laboratory conditions in radio frequency discharges, dust particles of about 5 μm diameter or larger are too heavy to be levitated by the weak ambipolar field inside the plasma volume. Rather, the particles sediment into the sheath region before an electrode, where the time-averaged electric field E is strong enough to balance the weight force when the Millikan condition $q_d E = m_d g$ is fulfilled (q_d and m_d being the dust charge and mass, and g the gravitational acceleration) [20].

Unlike the situation of Millikan's oil-drop experiment, the electric field is not homogeneous but increases linearly from the sheath edge towards the electrode and leads to a parabolic potential well that provides a stable vertical confinement (see Fig. 1(a)). Dust particles in this potential well have a resonance frequency $\omega_0 = (q_d n_i e / m_d \epsilon_0)^{1/2}$, which can be used to determine the dust charge q_d when the ion density n_i in the sheath and the particle mass m_d are known [21, 22]. Lateral confinement of the dust cloud can either be realized as a harmonic potential well, e.g., by a parabolic depression of the electrode surface, or as surface confinement, which is provided by a suitable barrier on the electrode that raises the equipotentials (see Figs. 1(b), (c)).

Dust confinement against gravity comes at a price. The plasma sheath is a region with a supersonic ion flow, $v_i > v_B$, where the ion velocity v_i exceeds the Bohm velocity $v_B = (k_B T_e / m_i)^{1/2}$ (T_e is the electron temperature and m_i the ion mass). This ion flow is responsible for anisotropic shielding of the dust and provides a source

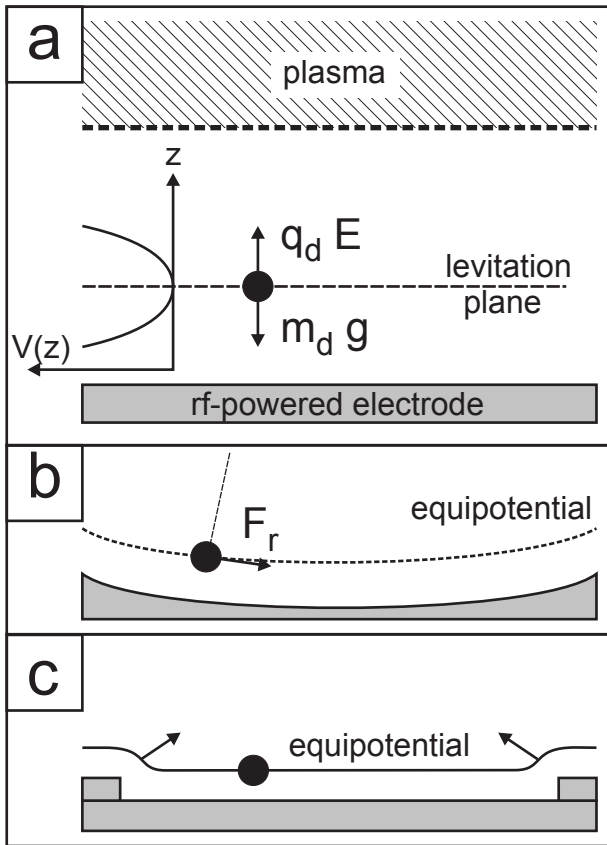


Fig. 1 (a) Levitation of a dust particle in the sheath. The inhomogeneous electric field leads to a vertical harmonic confinement. (b) Horizontal confinement by a parabolic shaped electrode. The restoring force F_r is proportional to the radial displacement. (c) Lateral confinement by barriers.

of free energy for instabilities. Dust clouds confined in such a potential trap can form monolayers or multilayer systems. The monolayers show a hexagonal order in the plane (Fig. 2(a)), which is the expected minimum energy configuration. A two-layer system (Fig. 2(b)) has a surprising aligned structure. This alignment is a consequence of the ion flow, which is deflected by the highly charged particle and forms an “ion focus” in the wake of the upper particle (see Fig. 2(c)) [23, 24]. The positive charge in the ion focus then attracts the lower particle. Long strings of particles can be formed in multilayer systems in rf discharges [17, 21, 25] or in dust clouds trapped in a striation of a dc-discharge, [26]. A detailed discussion of wakefield attraction can be found in Ref. [27].

Bulk order (fcc,bcc,hcp) was found in multilayer systems in the sheath region when the ion focus was destroyed by ion-neutral collisions at enhanced gas pressure [28, 29]. The high gas pressure prevented studying dynamic phenomena in these systems. A face-centered orthorhombic structure was reported for a cloud of very small particles (1.4 μm diameter) suspended in the quasineutral plasma [30]. Under microgravity, a region of the dust cloud

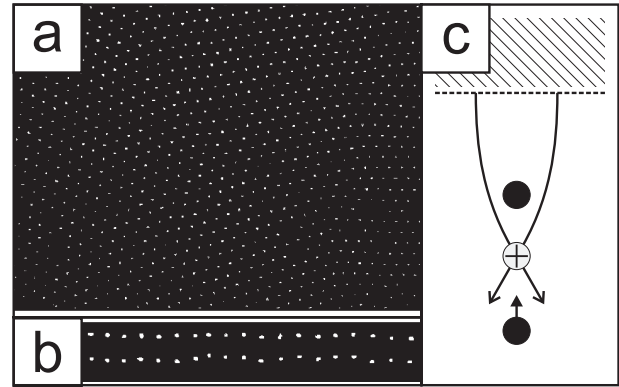


Fig. 2 (a) Top view of a two-layer plasma crystal. (b) Side view showing vertical alignment. (c) Deflection of the supersonic ion flow by the upper particle and formation of a positive net charge in the ion focus.

was found crystalline with domains of fcc, bcc, and hcp structure [31].

The interaction force between dust particles inside the levitation plane is a shielded Coulomb force. Collision experiments between pairs of particles showed that the pair interaction can be represented by a Yukawa potential

$$\phi(r) = \frac{q_d^2}{4\pi\epsilon_0 r} \exp\left(-\frac{r}{\lambda}\right) \quad (1)$$

with a shielding length $\lambda \approx \lambda_{De}$ that is close to the electron Debye length [32]. Unlike shielding in the bulk plasma, where the ion contribution to shielding is determined by the ion temperature, ion shielding by a supersonic flow involves the ion streaming energy, which exceeds $k_B T_e$. Therefore, the effective Debye length should be comparable to the electron Debye length. This interaction law was independently confirmed by analyzing the self-compression of a monolayer cluster in a parabolic trap [33].

The structure of finite 2D clusters was studied by stepwise increasing the number of particles in a monolayer. It was found that symmetric patterns and shell structures are formed [34, 35]. The enhanced stability of closed shells compared to incomplete shells was demonstrated by laser-excited intershell rotation [36].

Crystallization of the particle system requires that the coupling parameter Γ for screened interaction exceeds a critical value, $\Gamma_c = 175$ for three-dimensional systems

$$\Gamma = \frac{q_d^2}{4\pi\epsilon_0 a_{WS} k_B T_d} \exp\left(-\frac{a_{WS}}{\lambda}\right). \quad (2)$$

Here, $a_{WS} = (3/4\pi n_d)^{1/3}$ is the Wigner-Seitz radius, n_d the dust number density and T_d the dust kinetic temperature. The large value of $q_d = (10^3-10^4)e$ allows crystallization of the dust cloud at room temperature whereas trapped ions with $q = e$ require cooling to milli-Kelvins.

3. Waves in Monolayer Systems

The interparticle forces in a plasma crystal can be explored by exciting elastic waves. A monolayer supports compressional and shear modes in the plane, which have different sound speeds and a different dependence on the shielding length [37]. Measuring both sound speeds is a suitable method to determine q_d and λ . Wave experiments were restricted to monolayer plasma crystals, because multilayer systems are subject to the Schweigert instability [24, 38], which is fed by the free energy of the streaming ions and leads to violent oscillations and subsequent melting of the crystal. Compressional waves can be excited by the radiation pressure of a laser [39–41] and q_d and λ could be derived from dispersion and damping of the waves. The excitation of shear waves was introduced in Ref. [42]. Besides the study of plane waves, radiation from a point source was discussed in Ref. [43], and the localized shear was found to excite elastic vortex pairs. Instead of laser excited waves, the spectra of compressional and shear phonons can also be recovered by Fourier analysis of the thermal fluctuations of the particles [44]. Recent investigations were focussed on the modification of the phonon spectra near the melting transition [45]. Short wavelength shear waves in the liquid phase could be excited with a laser [46] and the expected long-wavelength cut-off for shear waves in the liquid phase was confirmed [47]. The nonlinear interaction of compressional phonons was observed above a threshold value that depends on frictional damping [48].

Instead of their wave dispersion properties, compressional and shear modes can be studied by exciting Mach cones. The first observation of Mach cones excited by fast out-of-plane particles [50] was accidental. Laser excitation of Mach cones was introduced in Ref. [51]. The half-angle μ of the Mach cone is related to the sound speed c_s by

$$\sin(\mu) = c_s/u, \quad (3)$$

where u is the velocity of the disturbance that generates the Mach cone. Wave dispersion outside the acoustic part of the dispersion branch leads to an internal interference structure of the Mach cone [52], which resembles the transverse and lateral wakes in the “Kelvin wedge” behind a moving ship in deep water. The simultaneous excitation of compressional and shear Mach cones and the corresponding wake structures were described in Ref. [49]. The resulting Mach relation [Eq. (3)] is shown in Fig. 3. The different sound velocities of the compressional and shear wave become evident from the different slopes of the fit lines, which is proportional to $1/c_s$. In this way, Mach cones can be used as a diagnostic tool for monolayer plasma crystals.

4. Yukawa Balls

Spherical plasma crystals were discovered in 2004 [53] when a cloud of dust particles was levitated by the thermophoretic force arising from a vertical tempera-

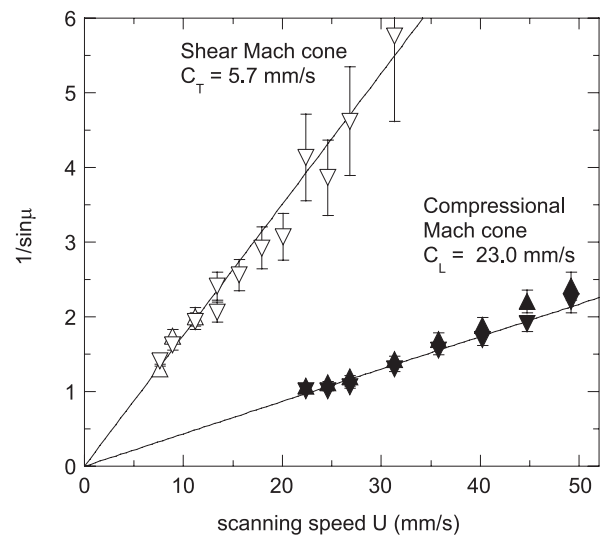


Fig. 3 Test of the Mach relation for compressional and shear Mach cones (from Ref. [49]).

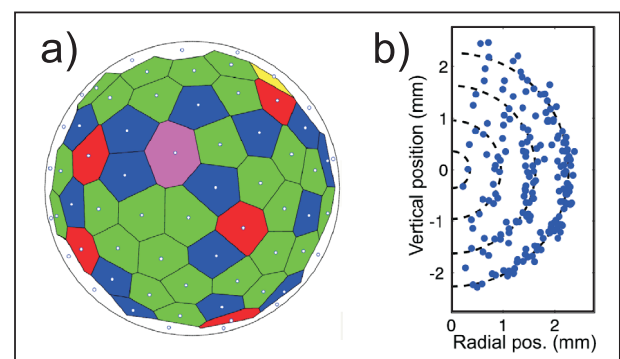


Fig. 4 (a) Particle arrangements in the outer shell of a Yukawa ball. The superimposed Voronoi cells show the expected hexagons and pentagons as well as defects. (b) Plotting all particle positions in cylindrical coordinates (ρ, z) reveals the shell structure (from [53]).

ture gradient in the gas, and was confined by nearby glass walls. These objects were coined “Yukawa balls” because of the shielded interaction of dust particles in a plasma and to distinguish them from laser-cooled ions that form Coulomb balls. Yukawa balls show a nested shell structure with mostly hexagonal order inside the shells (see Fig. 4). Three-dimensional dust clusters with a small number of particles confined in a plasmoid were reported in Ref. [54].

A detailed analysis of the force field [55] showed that Yukawa balls are confined in a spherical harmonic trap. Much insight into the building principles of Yukawa balls was gained from computer simulations of trapped particles that interact via a Yukawa potential [56–61].

4.1 Structure of Yukawa balls

Some of the differences between Yukawa and Coulomb balls can be understood by a simple model based on the different interaction force. Consider a spherical assembly of N particles each carrying a charge Q , which are confined in a parabolic potential well $V_t(r) = (1/2)\alpha r^2$ and interact pairwise either by a repulsive Coulomb force $F_C(r_{ij}) = Q^2/(4\pi\epsilon_0 r_{ij}^2)$ or by a shielded Yukawa force

$$F_Y(r_{ij}) = \frac{Q^2}{4\pi\epsilon_0 r_{ij}^2} \left(1 + \frac{r_{ij}}{\lambda}\right) \exp\left(-\frac{r_{ij}}{\lambda}\right) \quad (4)$$

with shielding length λ . The peculiarity of the Coulomb force is twofold: (a) Inside a hollow sphere there is no electric field and (b) a charge distribution with spherical symmetry can be replaced by a point charge at the center of the sphere (see Fig. 5(a)). The internal structure of a Coulomb ball is therefore determined by the requirement that each particle, at radial position r , is in a force balance between the repulsion from all those particles at positions $r_1 \leq r$ and the restoring force $F_t(r) = -\alpha r$ from the trap. When we assume that there are $N(r)$ particles inside the radius r , the force balance requires

$$\frac{[N(r) - 1]Q^2}{4\pi\epsilon_0 r^2} = \alpha r, \quad (5)$$

hence $[N(r) - 1] \propto r^3$. On the other hand, when we represent the discrete particle distribution by a continuous density distribution $n(r)$, we have

$$N(r) \approx 4\pi \int_0^r n(r_1) r_1^2 dr_1. \quad (6)$$

Hence, $dN(r)/dr = 4\pi n(r)r^2 \propto r^2$ can only be fulfilled for a constant density $n(r) = 3\alpha\epsilon_0/Q^2 =: n_C$. Therefore, a Coulomb ball in a parabolic trap is necessarily homogeneous. In particular, the radius of a Coulomb ball

$$R_C = \left[\frac{(N-1)Q^2}{4\pi\epsilon_0\alpha} \right]^{1/3} \quad (7)$$

can be obtained from the force balance of a particle at the surface.

For shielded interaction, these principles do not hold any longer. Consider a point charge Q at a distance $z - z_0$ from a homogeneously charged (infinitely large) plane of thickness dz and density $n(z_0)$ (see Fig. 5(b)). The test charge interacts with each volume element in this plane by the shielded force (4) and the resulting repulsive force becomes

$$dF_z(z) = n(z_0) \frac{Q^2}{2\epsilon_0} \exp\left[-\frac{z-z_0}{\lambda}\right] dz. \quad (8)$$

This force now depends on the distance from the plane, whereas the force would be constant for Coulomb interaction. This simple model approximates the interaction between a point charge and a spherical shell as long as $r \gg \lambda$.

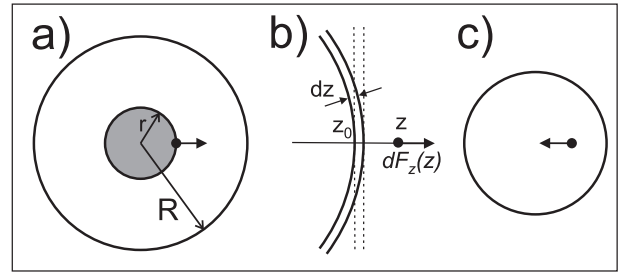


Fig. 5 (a) In a Coulomb ball, a particle experiences only a net force from shells with $r_1 < r$ while outer (hollow) shells give no net force. (b) The interaction of a particle with a shell of particles is approximated by the interaction with a charged plane. (c) In a Yukawa ball, a hollow shell exerts a net force on a particle that pushes it towards the center.

Moreover, because of the finite range of the Yukawa force, a particle in a hollow sphere, which is not at the center of the sphere, now experiences a net force that pushes it towards the center (see Fig. 5(c)). This is a first hint that Yukawa balls tend to have an inhomogeneous density profile.

A more quantitative description can be obtained for large Yukawa balls, which have $R/\lambda \gg 1$. The force equilibrium for a test particle of charge Q inside a Yukawa ball is defined by the balance of a net force from a gradient in the density $n(r)$ with the confining force F_t . For simplicity of calculation, we assume that the test particle is located between an inner and outer half space with a plane interface and a stratified set of density layers parallel to the interface, which have a density distribution $n(r_1) = n(r) + (r_1 - r)n'(r)$. Then, the force from the inner and outer half spaces become

$$\begin{aligned} F_{<} &= \frac{Q^2}{2\epsilon_0} [\lambda n(r) - \lambda^2 n'(r)], \\ F_{>} &= -\frac{Q^2}{2\epsilon_0} [\lambda n(r) + \lambda^2 n'(r)], \end{aligned} \quad (9)$$

which define the force balance

$$F_{<} + F_{>} = -\frac{Q^2}{\epsilon_0} \lambda^2 n'(r) = \alpha r. \quad (10)$$

Hence, for a parabolic confinement, the curvature of the density profile must be a constant,

$$n'' = -\frac{\alpha\epsilon_0}{Q^2\lambda^2} = -\frac{n_C}{3\lambda^2}. \quad (11)$$

Henning *et al.* [58] have shown, that the same result is obtained for a spherical geometry and for arbitrary R/λ . The density profile therefore has the shape of an inverted parabola,

$$n(r) = n(0) - \frac{1}{6} \frac{n_C}{\lambda^2} r^2. \quad (12)$$

The central density $n(0)$, however, still has to be determined.

The force balance at the surface of the Yukawa ball is determined by the balance from the inner half space with the trap, $F_z + F_t = 0$, which yields

$$\lambda n(R) - \lambda^2 n'(R) = \frac{2}{3} n_C R \quad (13)$$

and using $n'(R) = (1/3)n_C(R/\lambda^2)$ we obtain

$$n(R) = \frac{1}{3} n_C \frac{R}{\lambda}. \quad (14)$$

Therefore, despite the radial decay of the density, a Yukawa ball has a finite value of the particle density $n(R)$ at the surface. Finally, the density in the center of the Yukawa ball is obtained as

$$n(0) = \frac{1}{3} n_C \left[\frac{R}{\lambda} + \frac{1}{2} \frac{R^2}{\lambda^2} \right], \quad (15)$$

which gives the asymptotic form of the model in reference [58]. Note that the density at the surface scales $\propto R/\lambda$ but the central density increases more rapidly $\propto (R/\lambda)^2$. Hence, the larger a Yukawa ball becomes by adding more and more particles, the sharper peaked is the density profile in the center.

The total number of particles in a large Yukawa ball is given by

$$\begin{aligned} N &\approx \frac{2\pi}{3} \int_0^R n_C \left[\frac{R^2 - r^2}{\lambda^2} \right] r^2 dr \\ &= \frac{4\pi}{45} R^5 \frac{n_C}{\lambda^2}. \end{aligned} \quad (16)$$

For comparison, in a Coulomb ball, $N \approx (4\pi/3)R_C^3 n_C$. This leads to the useful relation $R/\lambda \approx 15^{1/5}(R_C/\lambda)^{3/5}$, which shows that, compared to a Coulomb ball, the growth of the radius of a Yukawa ball is much slower for the same number of particles.

The steepening of the profile shape can be seen in Fig. 6(a). There, the profile function from reference [58] is used with the asymptotic form $R/\lambda \approx 15^{1/5}(R_C/\lambda)^{3/5}$ and rescaled to an abscissa r/R_C . The shielding factor is here given as $R_C/\lambda = (N/2)^{1/3} r_0/\lambda$, r_0 being the equilibrium distance in the parabolic trap of two particles interacting by a Coulomb force. For $r_0/\lambda = 1$, the curves represent $N = 2000, 16000$, and 27000 particles.

The increase of the central density in a Yukawa ball by adding more and more particles to the system was studied experimentally and by computer simulation [57, 62]. The comparison is shown in Fig. 6(b). Here, the number of particles in the outermost shell becomes smaller than the prediction for a Coulomb ball (dashed line) whereas in the innermost shell, the population is larger than that of a Coulomb ball (full line). The population densities agree quite well with simulations for $r_0/\lambda = 0.6$. A density increase in the center could also be identified in experiments with small clusters [63].

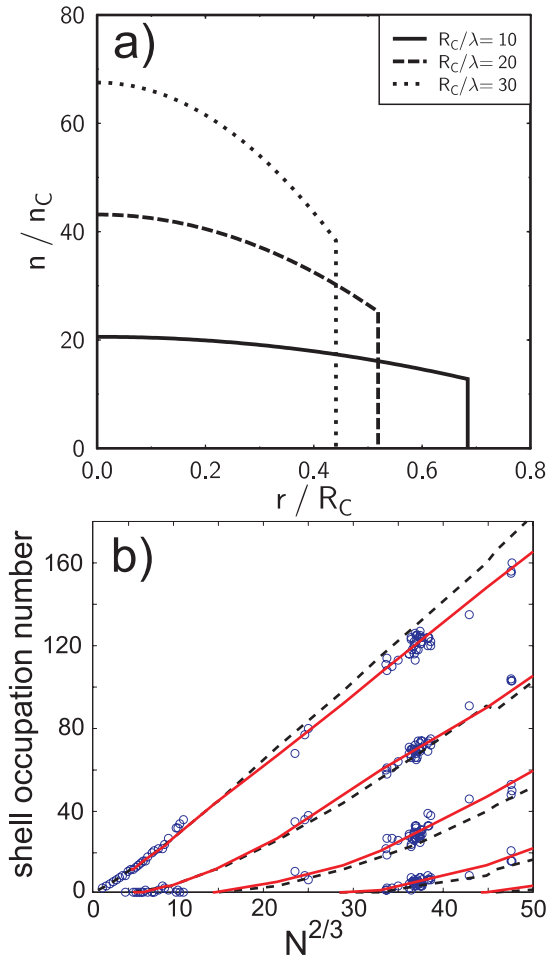


Fig. 6 (a) Density profiles of Yukawa balls for different values of R_C/λ . (b) Measured shell populations in comparison with the prediction for Coulomb balls (dashed line) and Yukawa balls for $r_0/\lambda = 0.6$ (full line).

4.2 Elastic properties of Yukawa balls

The elastic properties of Yukawa ball can be derived from the eigenmodes of the system, which are the analogon to the phonon dispersion in infinite systems. Eigenmodes of finite two-dimensional clusters were studied experimentally in Refs. [64, 65]. Usually, the mode of highest frequency is associated with the self-similar radial expansion (“breathing mode”). Recently, Henning *et al.* have proved that the breathing mode only exists for systems with power-law interaction or in Yukawa systems with special symmetries [66].

This can easily be seen from the following considerations. In the ground state, each particle at position \vec{r}_i in a Yukawa ball is in equilibrium with the confining force from the potential trap and with the repulsive forces from all other particles at a distance r_{ij} . In particular, the net torque for each particle is zero

$$\begin{aligned}
 0 &= \sum_{j \neq i} F(r_{ij}) \frac{\vec{r}_j - \vec{r}_i}{r_{ij}} \times \vec{r}_i \\
 &= \sum_{j \neq i} \frac{F(r_{ij})}{r_{ij}} (\vec{r}_j \times \vec{r}_i).
 \end{aligned} \quad (17)$$

Assuming now a small radial expansion of the Yukawa ball by a factor $D = 1 + \epsilon$, we obtain the condition

$$0 = \sum_{j \neq i} \frac{F(D r_{ij})}{D r_{ij}} (D^2 \vec{r}_j \times \vec{r}_i). \quad (18)$$

Requiring the arbitrariness of the \vec{r}_i , the interaction potential must fulfil the condition $F(Dr) = \beta F(r)$. Taylor expansion of F yields the differential equation

$$\epsilon r F'(r) - (\beta - 1)F(r) = 0, \quad (19)$$

which leads to a power-law shape of the interaction potential

$$F(r) = ar^c \quad \text{with} \quad c = (\beta - 1)/\epsilon. \quad (20)$$

The exponent c is usually negative but can even take positive values, as long as the confinement by the trap is ensured. Hence, a Coulomb ball with the r^{-1} interaction-law possesses a breathing mode, whereas for a Yukawa ball the self-similar radial expansion is not an eigenmode, except for some specific symmetric arrangements of particles. This shows again the difference between Coulomb and Yukawa balls, which originate from the different range of the interaction force.

5. Diagnostic Methods

The important difference between studying dynamic phenomena in 2D-plasma crystals and Yukawa balls is the necessity for a simultaneous measurement of the three spatial coordinates of all particles in the field of view. Different methods have been developed in the last few years for this purpose: the colour gradient method [54], the stereoscopy with an orthogonal arrangement of three cameras [67], and digital in-line holography [68].

In the colour gradient method, a small dust cloud is illuminated by two overlapping laser sheets of different colour with opposing intensity gradients along the line of sight of a camera system. The depth information is, in principle, contained in the intensity ratio of the scattered light, which is recorded by two cameras with the same field of view and appropriate colour filters. However, the depth resolution was found insufficient and most measurements with this system employed a third camera at right angle, which makes the arrangement a stereoscopic measurement system. With this system, small 3D dust clusters confined in a microplasma were studied with respect to the interaction force between the particles [69]. A detailed analysis led to the conjecture, that an attractive part of the interaction exists for interparticle distances $d \gg \lambda_D$, which by far exceed the linearized Debye length. This attractive part

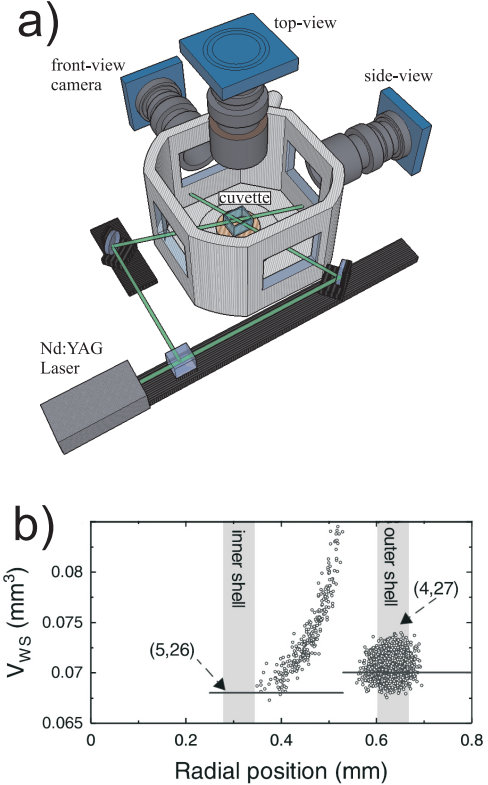


Fig. 7 (a) Arrangement of the cameras and the laser illumination for stereoscopic measurements (from [62]). (b) Change of the size of the Wigner-Seitz cells during a transition from metastable to ground state.

may be related to an unshielded dipole force that exceeds the shielded repulsive force at large distance [70]. In recent experiments, the normal modes of a small 3D cluster were investigated [71]. The spectrum shows a similarity with the eigenmode spectrum of a droplet, which was interpreted as a further hint at attractive forces which give the system a kind of surface tension.

The stereoscopic system with three orthogonal cameras was used to study the structure and dynamical processes of small Yukawa balls in a discharge of the kind used in Ref. [53]. Besides the ground state configurations of Yukawa balls, which had been studied with scanning video microscopy [57] the recent interest was focussed on metastable states [63]. In a large series of repeated experiments with clusters of $N = 31$ particles, the excited state (5,26) was found more often than the ground state (4,27), which can partly be attributed to the higher statistical weight of the metastable state [72]. In this system, the transition between ground state and metastable state could be followed dynamically by stereoscopy. This enabled a detailed analysis of the volume of the inner Wigner-Seitz cells during the transition (see Fig. 7), which become smaller for the inner shell. This supports the finding of inhomogeneous density profiles of Yukawa balls discussed

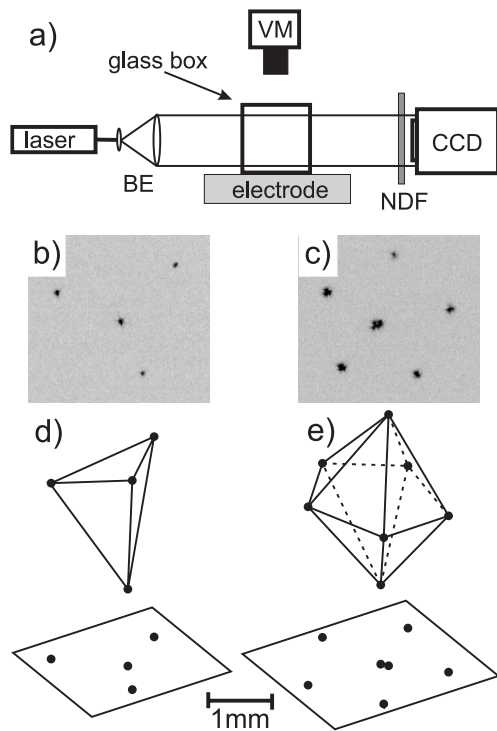


Fig. 8 (a) Experimental arrangement for digital in-line holography with laser, beam expander (BE), glass box containing the Yukawa ball, neutral density filter (NDF) and CMOS camera. (b,c) Images of ($N=4$) and ($N=7$) clusters from top-view video camera (VM). (d,e) Reconstructed 3D view with projections into the horizontal plane.

above.

Holography is in principle able to record the full spatial arrangement of a set of particles. Because of the finite pixel size in digital cameras, which are much larger than the silver grains in photographic plates for holography, digital holography is preferentially made in an in-line arrangement (DIH) (see Fig. 8(a)), which leads to smaller spatial frequencies in the interference pattern on the sensor.

Like all camera methods, there is little doubt about the lateral positions of the particles in the image plane. The challenge lies in the depth resolution. The DIH method was tested with small clusters of 4 or 7 particles (Figs. 8(b)-(e)), for which a direct comparison with a video microscope (VM in Fig. 8(a)) can be made. The reconstructed 3D images show an excellent agreement between DIH and VM positions.

6. Concluding Remarks

Finite 3D particle arrangements represent a new and interesting research topic in the field of complex plasmas. The new questions have stimulated the development of advanced diagnostic techniques. Significant progress has been achieved with respect to the structural and dynamical properties of 3D clusters. Because of the overwhelming number of publications in the field of plasma crys-

als, some interesting aspects had to be omitted from this overview, like phase transitions, transport properties, collisions of dust clouds or quantum effects. Some of these aspects were addressed in earlier reviews [73–75].

Fruitful discussions with D. Block and M. Bonitz are gratefully acknowledged. This work was supported by DFG within SFB-TR24 projects A2 and A3, and by DLR under grant 50WM0739.

- [1] J.J. Thomson, *Phil. Mag.* **39**, 237 (1904).
- [2] E. Wigner, *Phys. Rev.* **46**, 1002 (1934).
- [3] R.F. Wuerker, H. Shelton and R.V. Langmuir, *J. Appl. Phys.* **30**, 342 (1959).
- [4] W. Luck, M. Klier and H. Wesslau, *Ber. Bunsenges. Phys. Chem.* **50**, 485 (1963).
- [5] P.A. Hiltner and I.M. Krieger, *J. Phys. Chem.* **73**, 2386 (1969).
- [6] A. Kose, M. Ozaki, K. Takano, Y. Kobayashi and S. Hachiso, *J. Colloid Interface Sci.* **44**, 330 (1973).
- [7] R. Williams and R.S. Crandall, *Phys. Lett. A* **48**, 225 (1974).
- [8] F. Diedrich, E. Peik, J.M. Chen, W. Quint and H. Walther, *Phys. Rev. Lett.* **59**, 2931 (1987).
- [9] D.J. Wineland, J.C. Bergquist, W.M. Itano, J.J. Bollinger and C.H. Manney, *Phys. Rev. Lett.* **59**, 2935 (1987).
- [10] S.L. Gilbert, J.J. Bollinger and D.J. Wineland, *Phys. Rev. Lett.* **60**, 2022 (1988).
- [11] M. Drewsen, C. Brodersen, L. Hornekaer, J. Hangst and J. Schiffer, *Phys. Rev. Lett.* **81**, 2878 (1998).
- [12] A. Rahman and J.P. Schiffer, *Phys. Rev. Lett.* **57**, 1133 (1986).
- [13] J.P. Schiffer, *Phys. Rev. Lett.* **61**, 1843 (1988).
- [14] D.H.E. Dubin and T.M. O’Neil, *Phys. Rev. Lett.* **60**, 511 (1988).
- [15] D.H.E. Dubin and T.M. O’Neill, *Rev. Mod. Phys.* **71**, 87 (1999).
- [16] H. Ikezi, *Phys. Fluids* **29**, 1764 (1986).
- [17] J.H. Chu and L.I. Physica A **205**, 183 (1994).
- [18] Y. Hayashi and K. Tachibana, *Jpn. J. Appl. Phys.* **33**, L804 (1994).
- [19] H. Thomas, G.E. Morfill, V. Demmel, J. Goree, B. Feuerbacher and D. Möhlmann, *Phys. Rev. Lett.* **73**, 652 (1994).
- [20] A. Melzer, T. Trottenberg and A. Piel, *Phys. Lett. A* **191**, 301 (1994).
- [21] T. Trottenberg, A. Melzer and A. Piel, *Plasma Sources Sci. Technol.* **4**, 450 (1995).
- [22] A. Homann, A. Melzer and A. Piel, *Phys. Rev. E* **59**, 3835 (1999).
- [23] F. Melandsø and J. Goree, *Phys. Rev. E* **52**, 5312 (1995).
- [24] V.A. Schweigert, I.V. Schweigert, A. Melzer, A. Homann and A. Piel, *Phys. Rev. E* **54**, 4155 (1996).
- [25] K. Takahashi, T. Oishi, K. Shimomai, Y. Hayashi and S. Nishino, *Phys. Rev. E* **58**, 7805 (1998).
- [26] A.V. Zobnin, A.P. Nefedov, V.A. Sinel’shchikov, O.A. Sinkevich, A.D. Usachev, V.S. Filippov and V.E. Fortov, *Plasma Physics Reports* **26**, 415 (2000).
- [27] A. Piel, O. Arp, D. Block, I. Pilch, T. Trottenberg, S. Käding, A. Melzer, H. Baumgartner, C. Henning and M. Bonitz, *Plasma Phys. Control. Fusion* **50**, 124003 (2008).
- [28] J.B. Pieper and J. Goree, *Phys. Rev. Lett.* **77**, 3137 (1996).
- [29] M. Zuzic, A.V. Ivlev, J. Goree, G.E. Morfill, H.M.

- Thomas, H. Rothermel, U. Konopka, R. Sütterlin and D.D. Goldbeck, *Phys. Rev. Lett.* **85**, 4064 (2000).
- [30] Y. Hayashi, *Phys. Rev. Lett.* **83**, 4764 (1999).
- [31] A.P. Nefedov, G.E. Morfill, V.E. Fortov, H.M. Thomas, H. Rothermel, T. Hagl, A.V. Ivlev, M. Zuzic, B.A. Klumov, A.M. Lipaev *et al.*, *New J. Phys.* **5**, 33 (2003).
- [32] U. Konopka, L. Ratke and H.M. Thomas, *Phys. Rev. Lett.* **79**, 1269 (1997).
- [33] G.A. Hebner, M.E. Riley and K.E. Greenberg, *Phys. Rev. E* **66**, 046407 (2002).
- [34] V.M. Bedanov and F. Peeters, *Phys. Rev. B* **49**, 2667 (1994).
- [35] W.-T. Juan, Z.-H. Huang, J.-W. Hsu, Y.-J. Lai and L. I, *Phys. Rev. E* **58**, R6947 (1998).
- [36] M. Klindworth, A. Melzer, A. Piel and V.A. Schweigert, *Phys. Rev. B* **61**, 8404 (2000).
- [37] F.M. Peeters and X. Wu, *Phys. Rev. A* **35**, 3109 (1987).
- [38] A. Melzer, V. Schweigert, I. Schweigert, A. Homann, S. Peters and A. Piel, *Phys. Rev. E* **54**, R46 (1996).
- [39] A. Homann, A. Melzer, S. Peters, R. Madani and A. Piel, *Phys. Rev. E* **56**, 7138 (1997).
- [40] A. Homann, A. Melzer, S. Peters, R. Madani and A. Piel, *Phys. Lett. A* **242**, 173 (1998).
- [41] A. Piel, A. Homann and A. Melzer, *Plasma Phys. Control. Fusion* **41**, A453 (1999).
- [42] S. Nunomura, D. Samsonov and J. Goree, *Phys. Rev. Lett.* **84**, 5141 (2000).
- [43] A. Piel, V. Nosenko and J. Goree, *Phys. Rev. Lett.* **89**, 085004 (2002).
- [44] S. Nunomura, J. Goree, S. Hu, X. Wang, A. Bhattacharjee and K. Avinash, *Phys. Rev. Lett.* **89**, 035001 (2002).
- [45] S. Nunomura, S. Zhdanov, D. Samsonov and G. Morfill, *Phys. Rev. Lett.* **94**, 045001 (2005).
- [46] A. Piel, V. Nosenko and J. Goree, *Phys. Plasmas* **13**, 042104 (2006).
- [47] V. Nosenko, J. Goree and A. Piel, *Phys. Rev. Lett.* **97**, 115001 (2006).
- [48] V. Nosenko, K. Avinash, J. Goree and B. Liu, *Phys. Rev. Lett.* **92**, 085001 (2004).
- [49] V. Nosenko, J. Goree, Z.W. Ma, D.H.E. Dubin and A. Piel, *Phys. Rev. E* **68**, 056409 (2003).
- [50] D. Samsonov, J. Goree, Z. Ma, A. Bhattacharjee, H.M. Thomas and G.E. Morfill, *Phys. Rev. Lett.* **83**, 3649 (1999).
- [51] A. Melzer, S. Nunomura, D. Samsonov and J. Goree, *Phys. Rev. E* **62**, 4162 (2000).
- [52] D.H.E. Dubin, *Phys. Plasmas* **7**, 3895 (2000).
- [53] O. Arp, D. Block and A. Piel, *Phys. Rev. Lett.* **93**, 165004 (2004).
- [54] B.M. Annaratone, T. Antonova, D. Goldbeck, H. Thomas and G.E. Morfill, *Plasma Phys. Control. Fusion* **46**, B495 (2004).
- [55] O. Arp, D. Block, M. Klindworth and A. Piel, *Phys. Plasmas* **12**, 122102 (2005).
- [56] H. Totsuji, C. Totsuji, T. Ogawa and K. Tsuruta, *Phys. Rev. E* **71**, 045401 (2005).
- [57] M. Bonitz, D. Block, O. Arp, V. Golubnychiy, H. Baumgartner, P. Ludwig, A. Piel and A. Filinov, *Phys. Rev. Lett.* **96**, 075001 (2006).
- [58] C. Henning, H. Baumgartner, A. Piel, P. Ludwig, V. Golubnychiy, M. Bonitz and D. Block, *Phys. Rev. E* **74**, 056403 (2006).
- [59] C. Henning, P. Ludwig, A. Filinov, A. Piel and M. Bonitz, *Phys. Rev. E* **76**, 036404 (2007).
- [60] H. Baumgartner, H. Kählert, V. Golubnychiy, C. Henning, S. Käding, A. Melzer and M. Bonitz, *Contrib. Plasma Phys.* **47**, 281 (2007).
- [61] S. Apolinario, B. Partoens and F. Peeters, *New J. Phys.* **9**, 283 (2007).
- [62] D. Block, M. Kroll, O. Arp, A. Piel, S. Käding, A. Melzer, C. Henning, H. Baumgartner, P. Ludwig and M. Bonitz, *Plasma Phys. Control. Fusion* **49**, B109 (2007).
- [63] D. Block, S. Käding, A. Melzer, A. Piel, H. Baumgartner and M. Bonitz, *Phys. Plasmas* **15**, 040701 (2008).
- [64] A. Melzer, M. Klindworth and A. Piel, *Phys. Rev. Lett.* **87**, 115002 (2001).
- [65] A. Melzer, *Phys. Rev. E* **67**, 016411 (2003).
- [66] C. Henning, K. Fujioka, P. Ludwig, A. Piel, A. Melzer and M. Bonitz, *Phys. Rev. Lett.* **101**, 045002 (2008).
- [67] S. Käding and A. Melzer, *Phys. Plasmas* **13**, 090701 (2006).
- [68] M. Kroll, S. Harms, D. Block and A. Piel, *Phys. Plasmas* **15**, 063703 (2008).
- [69] T. Antonova, B.M. Annaratone, D.D. Goldbeck, V. Yaroshenko, H.M. Thomas and G.E. Morfill, *Phys. Rev. Lett.* **96**, 115001 (2006).
- [70] V.V. Yaroshenko, B.M. Annaratone, T. Antonova, H. Thomas and G. Morfill, *New J. Phys.* **8**, 203 (2006).
- [71] T. Antonova, B. Annaratone, H. Thomas and G. Morfill, *New J. Phys.* **10**, 043028 (2008).
- [72] H. Kählert, P. Ludwig, H. Baumgartner, M. Bonitz, A. Piel, D. Block and A. Melzer, *Phys. Rev. E* **78**, 036408 (2008).
- [73] G. Morfill, B.M. Annaratone, P. Bryant, A.V. Ivlev, H.M. Thomas, M. Zuzic and V.E. Fortov, *Plasma Phys. Control. Fusion* **44**, 263 (2002).
- [74] V.E. Fortov, A.V. Ivlev, S.A. Khrapak, A.G. Khrapak and G.E. Morfill, *Phys. Rep.* **421**, 1 (2005).
- [75] M. Bonitz, P. Ludwig, H. Baumgartner, C. Henning, A. Filinov, D. Block, O. Arp, A. Piel, S. Käding, Y. Ivanov *et al.*, *Phys. Plasmas* **15**, 055704 (2008).